Contact Angle and Contact Angle Hysteresis Measurements Using the Capillary Bridge Technique

ARTICLE *in* LANGMUIR · OCTOBER 2009

Impact Factor: 4.46 · DOI: 10.1021/la901616x · Source: PubMed

Langmuir Article

pubs.acs.org/Langmuir

Contact Angle and Contact Angle Hysteresis Measurements Using the Capillary Bridge Technique

Frédéric Restagno,* Christophe Poulard, Céline Cohen, Laurianne Vagharchakian,‡ and Liliane Léger

Laboratoire de Physique des Solides, Université Paris-Sud 11, UMR CNRS 8502, Bât. 510, Campus d'Orsay, F-91405 Orsay Cedex, France. ‡Present address: Inserm-CEA Cognitive Neuroimaging Unit, NeuroSpin Center, CEA/SAC/DSV/I2BM, F-91191 Gif/Yvette, France

Received May 6, 2009. Revised Manuscript Received July 16, 2009

A new experimental technique is proposed to easily measure both advancing and receding contact angles of a liquid on a solid surface, with unprecedented accuracy. The technique is based on the analysis of the evolution of a capillary bridge formed between a liquid bath and a solid surface (which needs to be spherical) when the distance between the surface and the liquid bath is slowly varied. The feasibility of the technique is demonstrated using a low-energy perfluorinated surface with two different test liquids (water and hexadecane). A detailed description of both experimental procedures and computational modeling are given, allowing one to determine contact angle values. It is shown that the origin of the high accuracy of this technique relies on the fact that the contact angles are automatically averaged over the whole periphery of the contact. This method appears to be particularly adapted to the characterization of surfaces with very low contact angle hysteresis.

Introduction

The contact angle of a liquid on a solid surface is a key parameter[1−3] that characterizes the wetting behavior important in several industrial processes as well as in our everyday life. It is not only indicative of how well a fluid wets a particular surface, but it can also be used to predict the penetration of liquids in porous structures,[4] the displacement of a fluid by another one,[5,6] or to characterize solid surfaces treatments. As an example, there has been a growing interest in the past for plasma treatments on polymer surfaces[7,8] or surface modifications in order to obtain superhydrophobic surfaces, which all have to be well characterized from the point of view of wettability.[9−12]

The contact angle is defined as the angle between the liquid−vapor and the solid−liquid interfaces, at the point where the three phases (solid, liquid, and gas) meet. At equilibrium, when this triple line is immobile, the equilibrium value θ_e of the contact angle is predicted to obey the familiar Young's equation,[1] which relates θ_e to γ, γ_{sl}, and γ_{sg}, which are, respectively, the liquid−gas, solid−liquid, and solid−gas interfacial tensions (or equivalently interfacial energies):

$$\cos\theta_e = \frac{\gamma_{sg} - \gamma_{sl}}{\gamma} \quad (1)$$

Clean glass and metals are good examples of high-energy surfaces on which most liquids spread spontaneously, as the right-hand side of eq 1 is larger than one, and the equilibrium contact angle is not defined. Polymer materials, such as Teflon or lucite, are typical examples of low-energy surfaces on which most liquids tend to form droplets with a rather large contact angle. A common task of chemical surface treatments is to change the chemical groups present at the surface of a given solid in order to manipulate the interactions at contact, affecting both γ_{sl} and γ_{sg} and thus the wettability of the solid by a given liquid. In some cases, as for example for treatments promoting adhesion, the wettability has to be increased, while in other cases, as for example for antifouling treatments, the surface energy needs to be reduced, producing surfaces on which most liquids do not spread.

Despite its apparent simplicity, eq 1 cannot easily be used to predict contact angle values. First, the interfacial tensions γ_{sl} and γ_{sg} cannot usually be measured directly. Second, real surfaces always contain heterogeneities of both chemical and geometrical (roughness) nature, which hardly allow one to measure the equilibrium contact angle correctly.[13−15] Indeed, when a liquid drop is deposited on a real surface, the contact angle depends on the way the liquid has evolved to produce the final immobile drop. When the drop has evolved through an expansion of the contact area, the angle is said to represent an "advancing" contact angle. When the drop has contracted, the angle is said to represent a "receding" contact angle. These angles are written θ_a and θ_r. Then, for any given solid/liquid contact, a range of contact angles may be found instead of a well-defined unique equilibrium value. This is the so-called hysteresis of the contact line. The difference between advancing and receding contact angles directly reflects the heterogeneities of a given surface, and is a key parameter to characterize surface treatments. In particular, a strong correlation between the roughness (geometrical and chemical) and the friction properties of a surface has been established recently for

*Corresponding author. E-mail: restagno@lps.u-psud.fr.

(1) de Gennes, P.-G. *Rev. Mod. Phys.* **1985**, *57*, 827–863.
(2) Adamson, A. W. *Physical Chemistry of Surfaces*, 5th ed.; Wiley: New-York, 1990.
(3) Marmur, A. *Colloids Surf., A: Physicochem. Eng. Aspects* **1996**, *116*, 55–61.
(4) Hui, M. H.; Blunt, M. J. *J. Phys. Chem. B* **2000**, *104*, 3833–3845.
(5) Wolf, F. G.; dos Santos, L. O. E.; Philippi, P. C. *Microfluid. Nanofluid.* **2008**, *4*, 307–319.
(6) Dobbs, H. T. *Phys. A* **1993**, *201*, 457–481.
(7) Chen, I. J.; Lindner, E. *Langmuir* **2007**, *23*, 3118–3122.
(8) Guruvenket, S.; Rao, G. M.; Komath, M.; Raichur, A. M. *Appl. Surf. Sci.* **2004**, *236*, 278–284.
(9) Erbil, H. Y.; Demirel, A. L.; Avci, Y.; Mert, O. *Science* **2003**, *299*, 1377–1380.
(10) Lafuma, A.; Quere, D. *Nat. Mater.* **2003**, *2*, 457–460.
(11) Feng, X. J.; Jiang, L. *Adv. Mater.* **2006**, *18*, 3063–3078.
(12) de Givenchy, E. P. T.; Amigoni, S.; Martin, C.; Andrada, G.; Caillier, L.; Geribaldi, S.; Guittard, F. *Langmuir* **2009**, *25*, 6448–6453.
(13) Extrand, C. W. *J. Colloid Interface Sci.* **1998**, *207*, 11–19.
(14) Léger, L.; Joanny, J. F. *Rep. Prog. Phys.* **1992**, *55*, 431–486.
(15) Tavana, H.; Neumann, A. W. *Adv. Colloid Interface Sci.* **2007**, *132*, 1–32.

various solid−liquid contacts, especially for quasi-smooth surfaces, which induce a very low friction and flow with slip at the wall.[16−19] It has been shown that this low friction was highly sensitive to tiny changes in the roughness of the surface at nanometric scales. These tiny details are hardly detectable by conventional surface characterization techniques, but do affect the contact angle hysteresis of a test liquid. It thus appears desirable to develop techniques to measure contact angles and contact angle hysteresis with a sensitivity and an accuracy that allows for a satisfying characterization of surfaces with very low contact angle hysteresis (1° or below). Such a task is hardly feasible with the presently available techniques, which are not sensitive enough. Among the various available contact angle measurement methods, the sessile drop and the Wilhelmy balance methods are the most widely used.[2] In the sessile drop method, the contact angle is directly read, using a goniometer, from the profile of a liquid droplet deposited on a flat sample.[20,21] The major advantages of this method are requirements of very small quantities of liquid and small test surfaces. Major disadvantages are a poor accuracy (uncertainties of several degrees, even if the accuracy can be improved by comparing the whole profile of the drop to the theoretically computed one) and a high sensitivity to surface contamination, since it leads to localized measurements at one point. In the Wilhelmy balance method, the contact angle is deduced from the force exerted by the liquid on a small plate or a ring, which is advanced to and/or receded from the liquid. The apparent weight of the plate (or ring) is measured, in the presence of the meniscus formed at the liquid−solid contact. The accuracy in terms of contact angles can be high since it relies on a force measurement, which can be performed with comparatively high accuracy, provided the weight of the meniscus is not negligible compared to the total weight (light samples like thin plates, thin fibers, or hairs). In the present paper, we describe an original optical technique that we have named the capillary bridge test, which allows one to measure both advancing and receding contact angles with an unprecedented accuracy, so that it can be used to characterize surfaces with low contact angle hysteresis (on the order of 1°). The potential of this new technique in terms of discriminating between low friction surface coatings (perfluorinated surfaces) has been reported in a recent paper.[22] The aim of the present paper is to describe how both advancing and receding contact angles can be quantitatively determined using the capillary bridge test, and to discuss its advantages and limitations compared to other available contact angle measurement techniques.

Experimental Methodology

Experimental Setup. The capillary bridge technique employs a transparent spherical surface (such as a watch glass used in chemistry laboratories) with a radius of curvature R of a few centimeters (in all the experiments presented here, $R = 100$ mm) and a liquid bath made of a cylindrical container with a transparent flat bottom that is filled with the test liquid. The diameter of the container is chosen much larger than the capillary length of the liquid so that the free surface of the liquid is essentially flat and horizontal before the formation of the capillary bridge. The capillary length κ^{-1} is the typical length scale above which gravity effects become important compared to capillary effects:

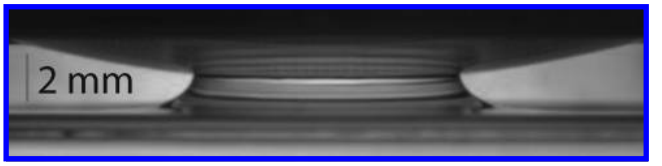

Figure 1. Liquid bridge formed between a spherical hydrophobic surface and a large bath of water. The surface is coated with a thin grafted perfluorinated polymer film, so that it is hydrophobic, with a contact angle for water larger than 90°.

$$\kappa^{-1} = \sqrt{\frac{\gamma}{\rho g}} \tag{2}$$

where γ is the liquid−gas surface tension, ρ is the density of the liquid, and g is the gravity constant. Usually κ^{-1} is a millimetric length ($\kappa^{-1} \simeq 2.73$ mm for water at room temperature). When the solid surface is brought into contact with the free surface of the liquid, a capillary bridge forms, with a finite area of contact of the liquid on the spherical surface, so that the liquid can touch the surface with the correct contact angle of the liquid on the spherical glass. We emphasize that the capillary bridge forms with a level of liquid at contact with the spherical surface higher than the rest level of liquid in the bath whatever the value of the contact angle on the surface (smaller or larger than 90°). As a result of the particular geometry of the system, only fully superhydrophobic surfaces with a contact angle equal to 180° can keep the liquid horizontal. Adhesion forces (wetting forces) associated with the creation of the wetted area of the solid are balanced by both the capillary forces associated with the curvature of the liquid−air interface and the gravity forces associated with the fact that inside the capillary bridge some liquid is raised above the free surface of the liquid bath. The formation of a capillary bridge by a liquid drop squeezed between two planar parallel surfaces has previously been investigated by Debrégeas et al.[23] who have shown that the meniscus was not always stable. We chose instead to form a capillary bridge between a large liquid bath and a spherical surface (Figure 1) for two reasons: first, the spherical surface with its axisymetric symmetry stabilizes the capillary bridge position and shape, allowing for an easy optical investigation; second, the large liquid reservoir allows the characteristics of the capillary bridge to be independent of the volume of liquid and only dependent on the characteristics of the spherical surface. It also facilitates the numerical resolution of the Laplace equation, which provides the shape of the capillary bridge by fixing a well-defined boundary condition: the liquid surface has to become horizontal far from the capillary bridge.

The capillary bridge is observed optically by two charge-coupled device (CCD) cameras (Sony XC-ST70CE, 752 × 582 pixels, 2/3″ sensor) equipped with a cosmicar TV zoom lens (12.5−75 mm) each. The first one is horizontal and monitors the profile of the capillary bridge (Figure 1). The second one is vertical and provides an image of the "wetted area" on the solid surface (which needs to be transparent). In fact, we measure the radius a of the wetted area and in the following sections of this article, we will call the "wetted area" the horizontal projection of the wetted area: πa^2. The solid can be pulled away or pushed toward the liquid bath at a chosen velocity V, and the evolution of the capillary bridge is examined as a function of the distance h between the apex of the solid surface and the liquid bath. The experimental setup is schematically described in Figure 2. In order

(16) Cottin-Bizonne, C.; Steinberger, A.; Cross, B.; Raccurt, O.; Charlaix, E. *Langmuir* **2008**, *24*, 1165–1172.
(17) Cottin-Bizonne, C.; Cross, B.; Steinberger, A.; Charlaix, E. *Phys. Rev. Lett.* **2005**, *94*, 056102.
(18) Schmatko, T.; Hervet, H.; Léeger, L. *Langmuir* **2006**, *22*, 6843–6850.
(19) Pit, R.; Hervet, H.; Leger, L. *Phys. Rev. Lett.* **2000**, *85*, 980–983.
(20) Kwok, D. Y.; Gietzelt, T.; Grundke, K.; Jacobasch, H. J.; Neumann, A. W. *Langmuir* **1997**, *13*, 2880–2894.
(21) Cabezas, M. G.; Bateni, A.; Montanero, J. M.; Neumann, A. W. *Langmuir* **2006**, *22*, 10053–10060.
(22) Vagharchakian, L.; Restagno, F.; Léger, L. *J. Phys. Chem. B* **2009**, *113*, 3769–3775.
(23) Debregeas, G.; Brochard Wyart, F. *J. Colloid Interface Sci.* **1997**, *190*, 134–141.

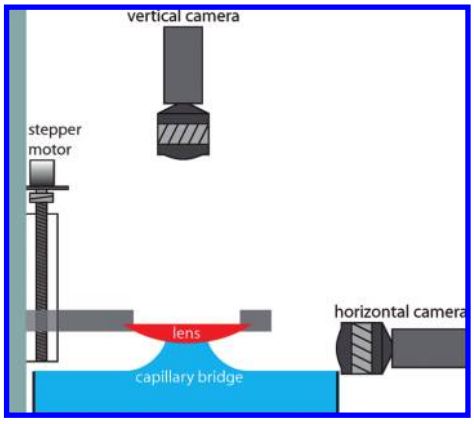

Figure 2. Experimental setup. The capillary bridge formed between a spherical lens and a large liquid bath is monitored through two synchronized cameras as a function of the distance between the bath and the lens.

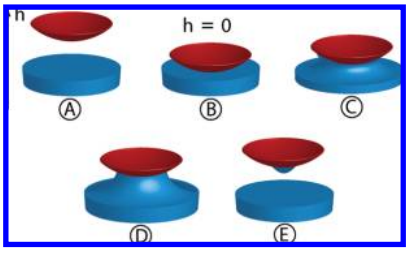

Figure 3. Schematic presentation of an experimental pulling sequence up to breakage: (A) approach of the surface to the liquid bath, (B) contact between the surface and the liquid, and (C) formation of the capillary bridge. (D) Withdrawal from of thesurface at chosen velocity, V, until the breakage of the capillary bridge. (E) After rupture, a droplet may remain attached to the surface.

to precisely control the position of the solid surface, a stepper motor (1.8°/step, Intelligent Motion System, M1719-1.5) is used, which is controlled by a microstep card (Intelligent Motion System, IMS-483). A microcontroller generates the TTL signal for the microstep card and sends the synchronization signal to a multichannel video acquisition card (Matrox, Meteor II-MC/4). LabVIEW software controls the entire experimental sequence. The parameters of the mechanical parts include a typical velocity range between 1 and 5000 μm/s, and an overall range of vertical displacements of 8 cm, with a resolution of 0.1 μm. The maximum images acquisition rate for the two cameras is 12 images/s/camera. A millimetric grid placed underneath the liquid bath allows for an easy quantification of the contact area.

The use of a large enough liquid bath (typical diameter of 20 cm) allows the capillary bridge to remain insensitive to the boundary conditions at the container walls. This is quite different from what would be observed for a capillary bridge formed between the spherical surface and a drop (with a small volume of liquid) deposited on a flat surface. Then, the shape of the capillary bridge would result from the competition of adhesion forces at the two surfaces, and thus be sensitive to the contact angles on both surfaces. With the large liquid bath, the behavior of the liquid bridge is determined by the contact between the spherical surface and the liquid.

Measurement Technique. A typical experiment proceeds as shown in Figure 3. The spherical surface, which is tightly fixed on the holder, slowly approaches the liquid bath with a velocity of about 1 μm/s when close to making the contact. The origin $h = 0$ is determined by the rapid formation of the liquid bridge when the spherical surface just touches the liquid surface. When care is taken to keep at a minimum the vibrations on the liquid surface, the accuracy of the determination of this origin is $\Delta h \simeq 1$ μm.

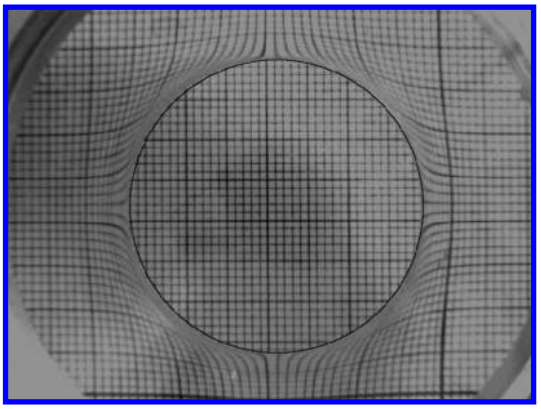

Figure 4. Typical picture obtained from the vertical camera showing the wetted area A. The millimetric grid placed below the liquid bath is optically distorted by the capillary bridge allowing for an easy visualization of the wetted area.

The solid surface is then withdrawn from the liquid bath at a velocity V. One can stop the pulling motion before the capillary bridge breaks, and reverse the motion, pushing the spherical surface back down to the liquid, and eventually describe push−pull cycles. Pictures of the contact area (as shown in Figure 4) allow one to measure the wetted area A, as a function of the displacement h.

It is important to notice that a careful adjustment of the lightening is necessary in order to obtain pictures with a sufficient contrast to allow for an automated treatment of the data. This was achieved with two diffuse light sources installed respectively below the liquid bath and opposite to the horizontal camera. A careful calibration of the scale also needs to be done in order to extract the wetted area (cm^2) from the pictures. Indeed, the millimetric grid is observed through the liquid bath and the curved spherical surface, with transverse magnification different from one, and depending on the total thickness of liquid between the glass and the bottom of the liquid bath. Along a full experimental cycle going from the formation of the capillary bridge to its breakage, this magnification can be considered as constant only if the range of displacement h remains small compared to the distance between the grid and the vertical camera. In all the experiments presented below, Newtonian liquids were used, leading to a maximal height of the capillary bridge not larger than 3 mm. The typical distance between the camera and the liquid bridge was typically 20 cm, so that the magnification variations could indeed be neglected. If larger displacements had been necessary, the vertical camera would have needed to be displaced with the solid surface in order to keep the magnification of the optical device constant during the experiment.

The wetted area can be extracted from the pictures using a simple program, such as ImageJ. In order to automate the measurements, a LabVIEW program has been developed, based on the correlation of two pictures. Since the changes in the grid pictures are localized at the rim of the wetted zone when the solid surface moves, the correlation of subsequent images in combination with a threshold analysis of the pictures allows one to precisely locate the edge of the wetted contact and determine the radius of the wetted area. A typical example of a treated image is presented in Figure 5.

The evolution with h of the shape of the capillary bridge is independent of the pull or push velocity, as long as V is kept small enough. The upper velocity limiting this quasi-static regime depends on the viscosity of the test liquid. For all the experiments reported in the present paper, this limiting velocity is close to 10 μm/s. For larger velocities, the evolution of the capillary bridge starts to depend on the velocity.[22] We do not discuss here the corresponding dynamical regime. In the quasi-static regime, after a given pull-off displacement, the motion can be reversed, and the

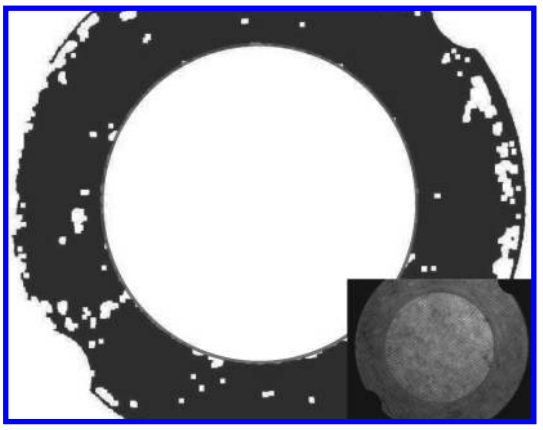

Figure 5. Threshold analysis of the pictures in order to automatically extract the wetted area from a raw picture (inset).

surface pushed toward the liquid. The evolution of the wetted area A as a function of the distance between the solid surface and the liquid bath, h, for these two sequences of motion (pull off and push back) contains the information on advancing and receding contact angles in a way that we shall now analyze in more detail. A typical example of the evolution of A versus the distance between the surface and the liquid bath, h, is given in Figure 6. Several independent experiments have been superimposed to emphasize the reproducibility of the experiment, and pull−push cycles have been performed.

As already reported in Vangharchakian et al.,[22] the $A(h)$ pull curves clearly display three regimes. For the example in Figure 6, focusing first on curves A to B1 to C, $A(h)$ remains constant for $h < 140\ \mu$m (part A), which means that the triple line remains pinned on the solid surface, at the location it took when the capillary bridge formed rapidly at $h = 0$. Then, for $140\ \mu\text{m} < h < 2140\ \mu$m (part B1), the wetted area decreases linearly as a function of h with a slope of 551 ± 1 mm. At larger distances (part C), a weak deviation from the linear behavior appears, associated with the proximity of the dynamical breaking process of the liquid bridge. The capillary bridge breaks at $h = h_f$. If the motion of the surface is reversed before h_f, focusing now on curves B2 and B3, the wetted area first remains independent of h (part B2: triple line pinned at the location it had when the motion was reversed), and then grows linearly when h decreases, following a curve B3 parallel but clearly distinct from the curve B1 obtained during the pull-off motion. If the motion of the surface is reversed again, a new plateau B4 is observed, and the wetted area rejoins curve B1.

Analysis of the $A(h)$ Curves

In this section, we develop both a simple analytical and a full numerical analysis of the evolution of the shape of the capillary bridge versus the pull-off distance h, which both provide a fundamental understanding of the experimental curves shown in Figure 6. In the next section, we shall show how one can use these analyses to get quantitative measurements of both advancing and receding contact angles of the liquid on the solid surface.

Meniscus calculations have been performed by a large number of researchers for many years. Fisher[24] analyzed the mean curvature of axisymetric menisci and the volume of trapped liquid. Woodrow et al.[25] solved the Laplace equation to obtain the profile of a meniscus formed between identical spheres. Orr et al.[26] solved the Laplace equation for a capillary bridge formed between a sphere and a flat surface. More recently, capillary bridges have received attention on a more dynamical point of view. Pitois et al.[27] calculated the rupture energy of a capillary bridge, and Cai and Bhushan[28,29] calculated the viscous and normal forces during the separation of different surfaces connected by capillary bridges. All these investigations were considering meniscus formed between two solids. In the capillary bridge technique discussed here, the capillary bridge connects a spherical solid and a liquid bath. The situation is axisymmetric and the only requirement for the liquid−air interface is to recover the flat surface of the liquid bath far from the capillary bridge. There is no restriction on the volume of liquid inside the capillary bridge itself.

Simple Analysis. One can understand the origin of the linear dependence of the experimental $A(h)$ curves and their dependence on the contact angle using a simple approximative argument. A scaling analysis shows that three length scales are present in the problem: the radius of curvature R of the surface, the capillary length κ^{-1}, and the radius a of the wetted area. Looking at the data in Figure 6, one can see that the capillary bridge remains stable at all distances between 0 and h_f, with h_f having the same order of magnitude as κ^{-1}. We also have $a \gg \kappa^{-1}$, except at the very end of the curve, near the breakage of the capillary bridge. This means that the axisymmetric curvature of the liquid−gas interface is almost always negligible in comparisons with the in-plane curvature as shown in Figure 7. As a consequence, the axisymmetric geometry can be neglected in a first approximation. Looking at Figure 7, one can estimate z_0, the height of the liquid above the level of the liquid bath, at the solid−liquid contact line, by analogy to the height of a meniscus on a vertical plate:[30]

$$z_0 = \kappa^{-1}\sqrt{2(1-\sin\beta)} \tag{3}$$

where β is the angle of the liquid with a virtual vertical plane at the triple line. β is related to the actual contact angle θ of the liquid on the real spherical surface through $\beta = \theta - \pi/2 + \alpha$. When the glass is pull up at a distance h from the liquid bath, a, z_0, h, and R remain related through the geometrical relation: $R^2 = a^2 + (R - (z_0 - h))^2$ (the equation of the spherical surface). Using $(z_0 - h) \ll R$, this gives

$$a^2 \simeq 2R(z_0 - h) \tag{4}$$

Combining eqs 3 and eq 4 leads to

$$A \simeq 2\pi R(\kappa^{-1}\sqrt{2(1+\cos(\alpha+\theta))} - h) \tag{5}$$

Since $\sin\alpha = a/R \ll 1$, we can neglect α in the previous expression, leading to

$$A \simeq 2\pi R(\kappa^{-1}\sqrt{2(1+\cos\theta)} - h) \tag{6}$$

which is valid for $R \gg \kappa^{-1}$ and if θ is not too small.

The linear relationship between the wetted area A and the distance from the liquid bath h thus results from a combination of a purely geometrical condition (the shape of the spherical surface) and the imposed contact angle at the surface. The slope of the $A(h)$ curves only depends on the radius of the spherical surface, while the absolute position of the $A(h)$ curve depends on θ and on the capillary length κ^{-1}. The experimentally determined $A(h)$ curves should thus allow one to quantify the contact angle, κ^{-1} being known for a given liquid. This simple approximate argument can be reinforced by a full numerical resolution of the Young−Laplace equation that we present now.

(24) Fisher, R. A. *J. Agric. Sci.* **1926**, *16*, 492–505.
(25) Woodrow, J.; Chilton, H.; Hawes, R. *J. Nucl. Energy B* **1961**, *2*, 229–37.
(26) Orr, F. M.; Scriven, L. E.; Rivas, A. P. *J. Fluid Mech.* **1975**, *67*, 723–742.
(27) Pitois, O. Ph.D. Thesis. École Nationale des Ponts et Chaussées, **1999**.
(28) Cai, S.; Bhushan, B. *Nanotechnology* **2007**, *18*, 465704.
(29) Bhushan, B.; Cai, S. *Appl. Mech. Rev.* **2008**, *61*, 050803.
(30) de Gennes, P.-G.; Brochard-Wyart, F.; Quéré, D. *Gouttes, bulles, perles et ondes*; Belin Edt.: Paris, 2005.

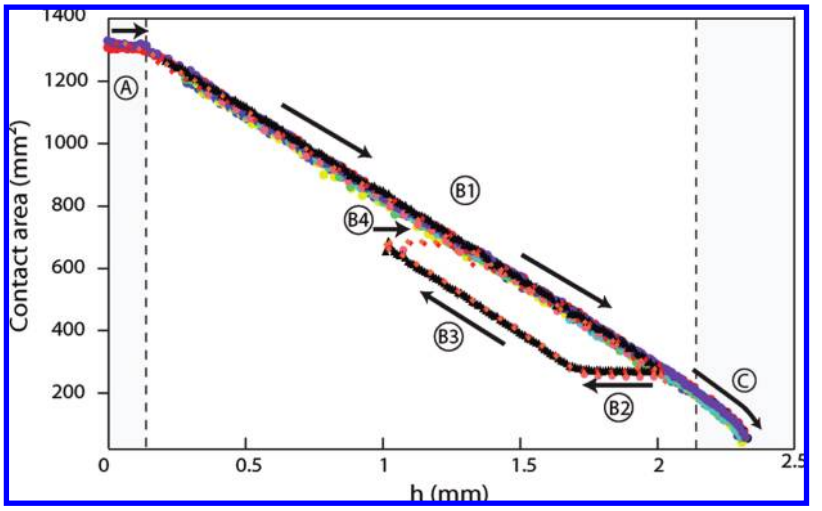

Figure 6. Typical experimental curves showing the evolution of the wetted area as a function of the distance h between a liquid bath of water and a solid surface covered with a perfluorinated thin polymer coating. The arrows indicate for each portion of curve, labeled successively A, B1, B2, B3, B4, and C, the way the curves were acquired, increasing (pull) or decreasing (push) h. The curve sections A, B1, B4, and C correspond to a pull-off sequence, while sections B2 and B3 correspond to a push-back one.

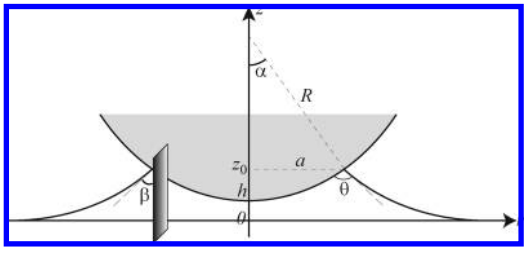

Figure 7. Schematic representation of a capillary bridge between a spherical surface and a large liquid bath, with the definition of the notations used in the analysis.

Numerical Analysis. The shape of the liquid−gas interface is governed by the Laplace equation, which relates the pressure drop across an interface to the interfacial tension and the two principle radii of curvature at the point of the liquid−gas surface under consideration. Using the notations introduced in Figure 7, this equation writes

$$\frac{\ddot{r}}{(1+\dot{r}^2)^{3/2}} - \frac{1}{r(1+\dot{r}^2)^{1/2}} = \frac{z}{\kappa^{-2}} \qquad (7)$$

where $\ddot{r} = d^2r/dz^2$ and $\dot{r} = dr/dz$. Contrary to several previous studies on the shape of a capillary bridge, we have chosen to work with the radial coordinates instead of with the arc length.[31,32]

Two initial boundary conditions are needed in order to solve eq 7. They are respectively the position r (z_0) of the edge of the capillary bridge on the spherical glass (triple line), and its first derivative $\dot{r}(z_0)$ at the same position. For a given distance z and a given contact angle θ, they are both fully defined by, respectively, the equation of the spherical surface and the geometry of the problem as specified in Figure 7:

$$\begin{cases} r(z_0) &= \sqrt{2R(z_0-h)-(z_0-h)^2} \\ \dot{r}(z_0) &= \cot(\theta+\alpha) \end{cases}$$

Equation 7 was first solved numerically using "MATLAB R2008a" and an explicit Runge−Kutta (4,5) method with chosen fixed values for the capillary length and the contact angle.

Then a series of $A(h)$ curves was numerically generated, varying the chosen value of the contact angle. Examples of such curves, for water as a test liquid, are reported in Figure 8 for contact angles varying by steps of 20° in the full possible range of contact angles, i.e., between 0 and 180°.

The overall shape of all the curves in Figure 8 appears to be in good qualitative agreement with the experimental data reported in Figure 6. First, all the numerical curves present a large range of linear decrease, with an average slope that is indeed very close to the experimental slope of the pull curves presented in part B1 in Figure 6. According to eq 5 this slope should be close to $2\pi R$ = 630 mm for water, which is indeed the case. Second, all numerical curves show deviations from the linear dependence, with an acceleration of the decrease in A, at their large h extremity, in a manner quite similar to that of the experimental data. The only difference between the experimental and numerical curves is the absence of any initial plateau in the numerically generated curves. This difference can easily be understood: the resolution of the Laplace equation gives the shape of the equilibrium capillary bridge for given h and θ. Experimentally, when the spherical surface is put into contact with the liquid bath, the capillary bridge forms rapidly, dynamical effects develop, and the experimental starting contact angle is close to an advancing contact angle. When the surface is pulled off the liquid bath, the wetted area cannot start to decrease before the contact angle has reached the receding contact angle. This is the origin of the initial plateau (A) in Figure 6: the wetted area remains fixed while h is increased, because the triple line is pinned on the surface, and can only start to move when the contact angle has decreased to the receding contact angle on this surface. Similarly, the plateau B2 that appears in Figure 6 when the motion of the surface is reversed and starts to be pushed down toward the liquid bath is also associated with the pinning of the triple line: the contact angle needs to increase from the receding up to the advancing contact angle before the wetted area can start to increase when decreasing h. As soon as the wetted area starts to evolve with h (either increasing or decreasing depending on the push or pull sequence considered), for the low velocity regime investigated here, the capillary bridge takes the $A(h)$ characteristics of an equilibrium

(31) Jennings, J. W.; Pallas, N. R. *Langmuir* **1988**, *4*, 959–967.
(32) del Rio, O. I.; Neumann, A. W. *J. Colloid Interface Sci.* **1997**, *196*, 136–147.

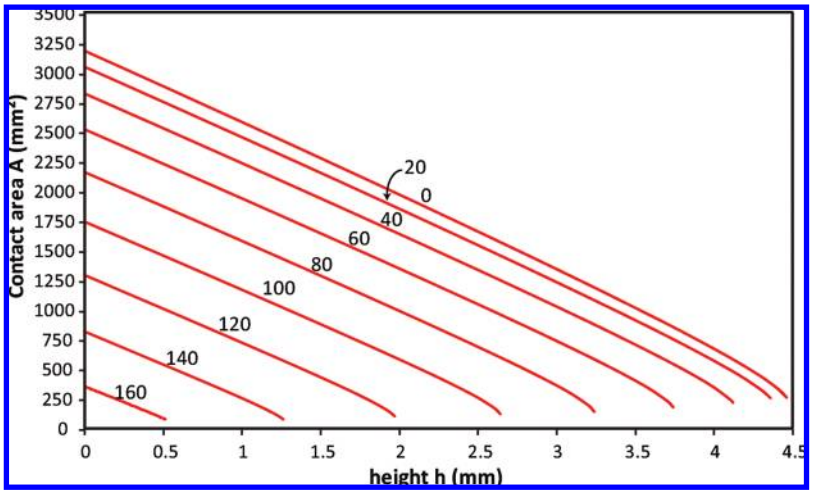

Figure 8. Numerically computed evolution of the wetted area A (in mm^2) as a function of h, the distance between the spherical surface and the liquid bath, for imposed values of the contact angle θ covering the full possible range 0° to 180°, by steps of 20°. All other parameters were fixed at their value for water: $\rho = 998$ kg·m^3, $\gamma = 72.8$ mN·m^{-1}.

capillary bridge, corresponding to the limiting contact angle on the surface, allowing for the motion of the triple line, i.e., the receding contact angle for a pull sequence or the advancing contact angle for a push sequence. It is well visible in Figure 8 that, as soon as the geometrical parameters of the surface and the capillary length of the liquid are fixed, the absolute position of any given $A(h)$ curve only depends on the contact angle. Then, both advancing and receding contact angle can be quantitatively determined respectively from the experimental $A(h)$ push and pull cycles by identifying which numerically generated curve can be superimposed with the experimental push or pull curves. We describe below the detailed procedure we propose to do so.

Quantitative Determination of Both Advancing and Receding Contact Angles from $A(h)$ Curves

The procedure to quantitatively determine receding contact angle from experimental $A(h)$ curves thus appears to be straightforward: one can look for the numerically generated curve that can be best superimposed on part B1 of the experimental $A(h)$ curve. This numerical curve gives the shape of the equilibrium capillary bridge obeying the various constraints of the problem: given capillary length, density of the liquid, and radius of the spherical surface, plus a contact angle on the surface that can be identified to the receding contact angle on that surface, provided the experimental curve has been acquired slowly enough to ensure quasistatic behavior. This latter condition can be checked experimentally by verifying that the experimental data do not depend appreciably on the pull velocity. The particular numerical curve that best superimposes with the pull section (B1 in Figure 6) can thus be used to identify the value of the receding contact angle. Similarly, identifying the numerical curve that can best be superimposed to section B3 of the experimental data in Figure 6 will allow for a quantitative determination of the advancing contact angle. Because the evolution of the wetted area as a function of h is essentially a straight line, with a slope fixed by the radius of curvature of the spherical surface, one can further simplify this identification of advancing and receding contact angles: the absolute position of any numerical curve in the $A(h)$ plane is fully determined by the corresponding initial contact area A_0. From the series of curves presented in Figure 8, one can generate a numerical curve $\theta = f(A_0)$, as reported in Figure 9 (for the set of parameters corresponding to water, and a radius of the surface

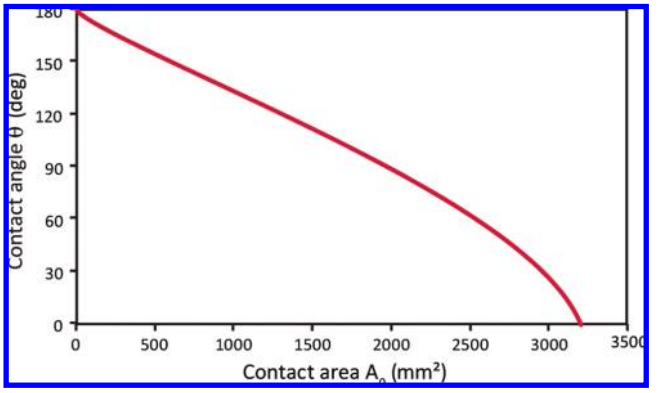

Figure 9. Evolution of the value of the contact angle θ as a function of the numerically computed initial wetted area $A_0 = A(h = 0)$, as deduced from the data corresponding to Figure 8. The other parameters were fixed at their value for water: $\rho = 998$ kg·m^3, $\gamma = 72.8\times$ mN·m^{-1}.

$R = 10$ cm). Figure 9 directly allows one to easily deduce both advancing and receding contact angles from the $A(h)$ cycles: by extrapolating both pull-off and push-back sections B1 and B3 shown in Figure 6 toward $h = 0$, the initial wetted areas of the equilibrium capillary bridges respectively having the receding and advancing contact angle on that given surface can be read, and used to translate in terms of contact angle values through Figure 9. It appears that even a contact angle hysteresis on the order of 1° is able to produce push and pull curves well separated from each other. This is what makes the technique quite well suited to quantify small contact angle hysteresis.

We discuss here the sensitivity of this method. A first question is to determine whether the simple analysis neglecting the curvature of the solid surface can be used instead of the full numerical analysis to produce the contact angle versus initial wetted area curve. Equation 6 gives an approximated initially wetted area, $A_0 = 2\pi R\kappa^{-1}[2(1 + \cos\theta)]^{1/2}$. In Figure 10, exact numerically calculated initial wetted areas, A_0, divided by $[2(1 + \cos\theta)]^{1/2}$ are reported as a function of the radius of curvature of the surface, for various contact angles, θ. The dotted line represents eq 6. It appears clearly that the simple analysis only works at very large radii of curvature for the spherical lens (above 1 m). For radii of curvature smaller than 1 m, the full numerical analysis is necessary.

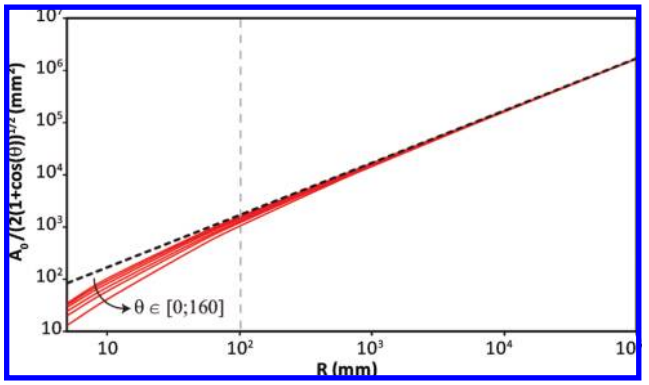

Figure 10. Solid lines: log−log plot of numerically computed evolutions of the initial wetted area $A_0 = A(h = 0)$ normalized by $2[(1 + \cos\theta)]^{1/2}$ as a function of the radius of curvature of the spherical surface R for different contact angles in the interval $\theta \in [0,160]$. The other parameters were fixed at their value for water: $\rho = 998\ \mathrm{kg\cdot m^3}$, $\gamma = 72.8\ \mathrm{mN\cdot m^{-1}}$. Dotted line: log−log plot of the evolution of initial wetted area A_0, as estimated by eq 6, again normalized by $2[(1 + \cos\theta)]^{1/2}$ versus the radius of curvature of the spherical surface R.

For example, for $R = 100$ mm, the relative deviation between simple and full analysis varies from 10% to 40% for contact angles θ in the range [0,160]°.

Sensitivity and Accuracy. As for any measurement technique, the questions of accuracy and sensitivity need be discussed. "Sensitivity" can be seen as the ability to differentiate fluctuations in a given observed or tested event. Here it is the ability to differentiate between close A_0 values. A first source of errors comes from the determination of the wetted area. The radius of the wetted area can be estimated to be known with an accuracy of ±1 pixel, which translates into ± 0.2 mm, with the optical magnification used in the present experiment. For a typical wetted area of 1000 mm^2, the corresponding uncertainty is 40 mm^2. Using the simplified eq 6, the sensitivity of the technique can be evaluated by

$$\frac{\Delta A_0}{\Delta\theta} \simeq 2\pi R\kappa^{-1} f(\theta) \qquad (8)$$

where f is an angular function of order 1. Using an uncertainty of the contact area of 40 mm^2, one gets an uncertainty on θ of 1.3°. This would indeed be the uncertainty on the contact angle if only one measurement of the contact area was performed for one particular h value. In fact, the technique easily provides a full $A(h)$ cruve, and A_0 is deduced using a linear fit on a large number of data points. The sensitivity is then much better than the above 1.3° estimate and will depend on the exact number of data points used in the fitting and extrapolation procedure. A second source of error is related to the uncertainty in the absolute position of the surface with respect to the rest level of the liquid bath. A position uncertainty (due essentially to the zero uncertainty) of $\Delta h = 1\ \mu$m gives an uncertainty of the contact area of $\Delta A_0 \simeq 2\pi R\Delta h \simeq 0.6$ mm^2. The corresponding error on the contact angle is negligible compared to that due to the quantification of the wetted area.

In practice, using a full $A(h)$ curve, we have shown experimentally that the repeatability of the experiment is better than 0.1° as a result of the automated statistical treatment. This appears to be 1 order of magnitude better than that for more conventional contact angle measurement methods.

Discussing the accuracy of the technique is more difficult since it depends on the numerical simulations. The main disadvantage of the capillary bridge technique, compared to a direct technique is that it necessitates a precise knowledge of the density and the surface tension of the liquid, and also of the radius of curvature of the solid surface. The comparison between a direct measurement and the capillary bridge technique needs to be experimental, as discussed below.

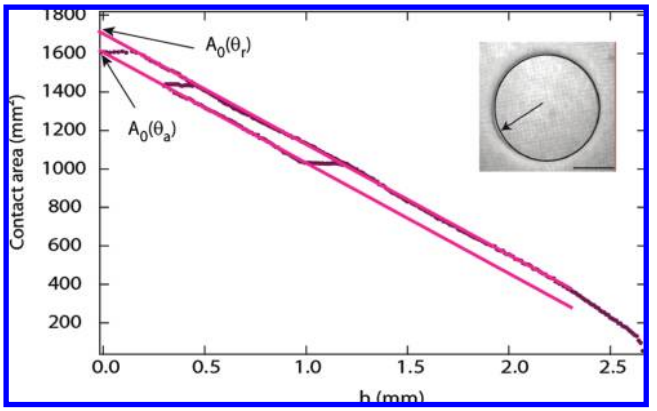

Figure 11. Comparison between experimental (markers) and numerical curves (continuous line) for hexadecane for both pull and push sequences. The different gray levels of the markers are related to different realizations of the experiment. The two initially wetted areas A_0 (θ_r) and A_0 (θ_a) allow to identify the receding and advancing contact angles, $\theta_r = 62.1°$ and $\theta_a = 70.0°$, respectively.

Application. *Materials*. In order to directly test the accuracy of the capillary bridge technique, two liquids have been used: deionized water (Millipore Milli-Q, resistivity $10^{18}\ \Omega\cdot$cm, surface tension = 72.8 mN/m, density = 0.998 g·cm^{-3}), and one low volatile alkane: hexadecane (surface tension = 27.4 mN/m, density = 0.770 g·cm^{-3}).

The surfaces were spherical watch glasses with a radius of curvature $R = 100$ mm, covered by a perfluorinated coatings described in more details in ref 22. The advancing and receding contact angles for water and hexadecane on these surfaces, as measured using the sessile drop method, are reported in Table 1.

Contact Angle Measurements. Let us focus first on hexadecane data. Typical push and pull cycles are reported in Figure 11.

Advancing and receding contact angles are deduced by identifying both advancing and receding initial contact areas, A_{0a} and A_{0r}, respectively, and then reading the values of the advancing and receding contact angles from a numerically generated $\theta(A_0)$ curve, similar to that presented in Figure 9, but now obtained inserting the parameters of hexadecane. As can be seen in Figure 11, one numerical $A(h)$, calculated for the tabulated values of hexadecane and the value $\theta = 62.1°$, perfectly superimposes the experimental data (square dots)), up to $h = 1.1$ mm for the pull curve (receding contact angle), while the numerical $A(h)$ curve, calculated with $\theta = 70.0°$ corresponds well to the push part of the experimental curve. The uncertainty in the determination of the initial wetted area leads to an uncertainty in the values of the contact angles of 0.1° in both cases. We emphasize that the experiment has been repeated five times, showing a quite high reproducibility. This mean that one can be confident in the values of both advancing and receding contact angles thus obtained.

Table 1. Advancing and Receding Contact Angles Values, Measured by the Conventional Sessile Drop Method on the Perfluorinated Surface

	θ_a	θ_r
water	117 ± 1.4°	113 ± 1.5°
hexadecane	70 ± 2°	64 ± 2°

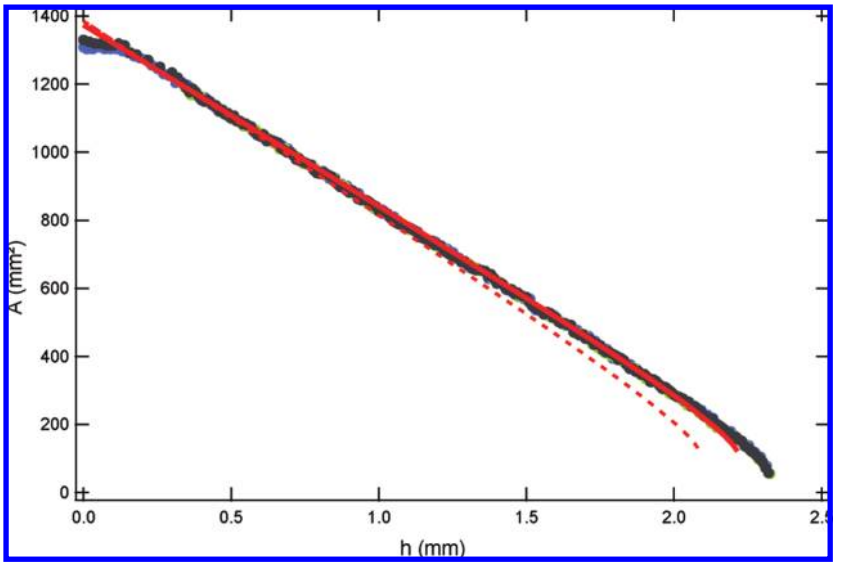

Figure 12. Comparison between experimental (markers) and numerical curves (lines) for water. The different gray levels of the markers are related to different realizations of the experiment. The thin dashed line is without the evaporation correction, and the solid thin line is calculated using a constant evaporation rate.

The value of 62.1° for the receding contact angle is slightly smaller than the 64° reported in Table 1. This is an example of the main advantage of the capillary bridge technique compared to the sessile drop technique: when a drop is deposited on a surface, one cannot ensure that the contact angle is either the advancing or the receding contact angle, except if one keeps slowly increasing or decreasing the volume of liquid inside the drop. To do so, a needle needs to remain inserted in the drop, which usually distorts the shape of the drop, and makes the determination of a contact angle more complicated. This is not the case with the capillary bridge technique, which automatically gives advancing and receding contact angles, provided that the push and pull sequences are performed at low enough velocities to guarantee a quasi-static capillary bridge for each h value. In Figure 11, slight deviations between the experimental data and the numerical pull curves appear for large h ($h > 1.2$ mm). These deviations have been correlated to a distortion of the contact area as shown in the insert of Figure 11. The observed pinning of the triple line is due to wetting heterogeneities of the surface, which can be easily detected by the capillary bridge technique, while they would have been difficult to put into evidence with a more conventional technique using localized small drops. This example demonstrates a second important advantage of the capillary bridge technique: by combining in a single experiment a high sensitivity and an easy span of the whole surface to be tested, the capillary bridge technique allows one to detect tiny local variations in surface treatments, which would have been quite difficult to trace back with other methods such as sessile drops, for example.

In the course of the different tests we have performed to test this new technique, we have been faced with a possible artifact that one needs to be aware of, which we shall now exemplify with the case of water. Typical pull curves are reported in Figure 12.

Again, several experiments have been performed to test the reproducibility of the technique. All experimental points are well collapsed in a single curve, but now the numerical curve best superimposed with the experimental data points at small h shows a noticeable deviation from the experiments for h larger than 1 mm. We have attributed this deviation to the evaporation of water. Indeed, on the time scale of a full h scan (around 30 min if one wants to remain in the quasi-static regime for the capillary bridge), evaporation of the test liquid may induce a progressive noticeable shift of the rest level of the liquid bath, inducing a bias in the assumed h values. Such an effect does not affect the value of the initial wetted area A_0, and one can obtain the receding contact angle $\theta = 116.9°$, in good agreement with the value reported in Table 1, but reducing the total number of data points that can be used to obtain the initial wetted area reduces the accuracy. This effect of evaporation can indeed be accounted for using, for example, the side view of the capillary bridge in order to couple the wetted area measurements to absolute values of the corresponding h. For the particular data reported in Figure 12, a constant evaporation rate of $\varepsilon = 70$ nm/s allows one to fully superimpose the numerical $A(h)$ curve to the experimental points, as shown by the solid line in Figure 12.

Conclusion

In this article, a new technique has been proposed that allows one to quantitatively determine both advancing and receding contact angles of various liquids on solid surfaces, with an unprecedented accuracy. As in the capillary rise test, which is widely used to measure surface tensions, the deformation of a liquid surface from horizontality is used to characterize the surface properties of a solid. Inspired by the now widely used JKR test,[33] the surface to be studied (which needs be spherical) is put into contact with a liquid bath in such a way that a capillary bridge forms that is connected to the solid via a circular triple line, defining a wetted area on the solid surface. Pulling the surface away from the bath allows one to progressively deform this capillary bridge. Monitoring the evolution of the wetted area with pull-off distance yields quantitative information on the receding contact angle of the liquid on the surface. Pushing back the surface toward the liquid bath allows one to quantitatively determine the advancing contact angle. At sufficiently small enough pull-off or push-back velocities, dynamical effects on the contact angle can be avoided, and the evolution of the capillary bridge can be considered quasi-static. In this regime, the wetted area varies linearly with distance. The absolute position of

(33) Johnson, K. L.; Kendall, K.; Roberts, A. D. *Proc. R. Soc. London, Ser. A: Math. Phys. Sci.* **1971**, *324*, 301–313.

this straight line is fixed by the value of the corresponding contact angle of the liquid on the surface (receding or advancing), which needs to be reached to allow the triple line to start gliding on the surface.

The experimental setup has been presented in detail, along with a numerical analysis, based on the numerical resolution of the Laplace equation giving the equilibrium shape of the capillary bridge, and thus the size of the wetted area on the solid surface. For a qualitative understanding of the experiment, an analytic approximation for solid surfaces with a low curvature has been proposed. It has also been shown that one could use the numerically computed values of the initial wetted area ($h = 0$) for a precise determination of both advancing and receding contact angles. Since the measurement process involves the displacement of the triple line on the large part of the solid surface, we emphasize that this method, contrary to other available contact angle measurement methods, gives values of the contact angle of the liquid on the surface that are automatically averaged over the whole periphery of the contact. Possible deviations of the measured wetted area versus distance curves from a straight line can be directly connected to the presence of wetting heterogeneities on the surface. This new method has been compared to the classical sessile drop method, showing quantitative agreement in the case of nonvolatile liquids. A possible artifact, related to the evaporation of the liquids has been pointed out, and possible ways of quantitatively correcting for evaporation effects have been proposed.

The capillary bridge technique could also be employed to measure dynamic contact angles. Then, as reported in the work of Vagharchakian et al.,[22] the shape of the capillary bridge deviates from the static one as a result of a dynamic wetting transition close to the contact line that is very similar to the Landau−Levich transition in the case of partial wetting.[34−36] A full analysis of these dynamic regimes will be presented in a forthcoming paper.

Because of its high sensitivity and convenient geometry, the presented technique could be used as a routine test in industry as well as in the laboratory. Moreover, it may provide answers to open fundamental questions such as, What governs the difference between advancing and receding contact angles at the molecular scale? What causes the pinning of a triple line, and What is the relationship between wetting, adhesion and friction? Model surfaces with controlled defects, or well-defined molecular organization could be used in the capillary bridge test to investigate these questions with accuracy.

Acknowledgment. We are deeply indebted to G. Josse who suggested to us the potential interest of the capillary bridge test. We want to thank E. Raphael, H. Hervet, A. Aradian, and T. Vilmin for valuable discussions on the modeling of the present experiment. We also thank P. Lacan and G Baillet from Essilor for financial support. We thank D. Brunello, V. Klein, S. Saranga and F. Saiag for their technical help in developing the experimental setup, and Dr. W. Drenckhan for her careful reading of our manuscript. Finally, C.C. acknowledges the Triangle de la Physique for a Ph.D. grant.

(34) Delon, G.; Fermigier, M.; Snoeijer, J. H.; Andreotti, B. *J. Fluid Mech.* **2008**, *604*, 55–75.
(35) Maleki, M.; Reyssat, E.; Quéré, D.; Golestanian, R. *Langmuir* **2007**, *23*, 10116–10122.
(36) Golestanian, R.; Raphael, E. *Europhys. Lett.* **2001**, *55*, 228–234.